Bias correction of extreme values of high resolution climate simulations for risk analysis.

luis Augusto sanabria (✉ LASF1327@gmail.com)
Ton Duc Thang University   https://orcid.org/0000-0002-9876-4660

Xuerong Qin
Guy Carpenter & Company

Jin Li
Data2Action

Robert Peter Cechet
University of New South Wales, Australian Defence Force Academy

---

Abstract

Most climatic models show that climate change affects natural perils' frequency and severity. Quantifying the impact of future climate conditions on natural hazard is essential for mitigation and adaptation planning. One crucial factor to consider when using climate simulations projections is the inherent systematic differences (bias) of the modelled data compared with observations. This bias can originate from the modelling process, the techniques used for downscaling of results, and the ensembles' intrinsic variability. Analysis of climate simulations has shown that the biases associated with these data types can be significant. Hence, it is often necessary to correct the bias before the data can be reliably used for further analysis.

Natural perils are often associated with extreme climatic conditions. Analysing trends in the tail end of distributions are already complicated because noise is much more prominent than that in the mean climate. The bias of the simulations can introduce significant errors in practical applications. In this paper, we present a methodology for bias correction of climate simulated data. The technique corrects the bias in both the body and the tail of the distribution (extreme values). As an illustration, maps of the 50 and 100-year Return Period of climate simulated Forest Fire Danger Index (FFDI) in Australia are presented and compared against the corresponding observation-based maps. The results show that the algorithm can substantially improve the calculation of simulation-based Return Periods. Forthcoming work will focus on the impact of climate change on these Return Periods considering future climate conditions.

1. Introduction

Numerous studies have shown that long term changes in weather patterns increase the frequency of natural hazards and seriously affect the lives of communities and regions (Ibarrarán et al. 2009; Van Aalst 2006). A critical role of governments is to work to restore ecosystems wherever possible and support communities to adapt to the changes as they occur. Plans for both mitigation and adaptation are vitally important for this process. Governments regularly use high-resolution projections downscaled from global climate simulations to devise these plans. (Orr et al. 2021). Recently communities have shown more and more interest in regional climatic projections. One of the central challenges facing scientists today is producing accurate and detailed high-resolution simulations (Handmer et al. 1999). Since climate simulations regularly feature coarse resolution and inaccuracies, researchers must continue developing strategies for downscaling and bias correction to ensure high-quality outcomes. (Bordoy, 2013).

The writers of this report will provide a technique to assist in the correction of bias in extreme values of climate simulations. Our goal is to improve the models we use to examine the effect of changing global climate on natural hazards by removing the inaccuracies in these extreme values. One example of a natural hazard that regularly impacts Australia is bushfires, also known as wildfires. Bushfires have occurred naturally in Australia for centuries, but their size and effect have been far from average over recent years. They have caused the destruction of vast areas of Australia and the death of millions of animals and some people (Abram et al. 2021). The area most affected has been the coastal fringe in south eastern Australia where population density is highest. The Australian Department of Home Affairs reported that, over the summer of 2019–2020, more than 12.6 million hectares of land across Australia were catastrophically burned; resulting in a $2.325 billion insured loss (Insurance Council Australia, 2020). 2019 was the hottest year ever recorded in Australia (Abram et al 2021) and changes to weather patterns are partly responsible for these devastating fires.

The south eastern coastal regions of Australia enjoy a mostly mild climate, with hot, dry summers and wet winters; however, the late summer period is often a time of extreme fire danger. The rains of spring and summer promote extensive plant growth, and the dryness of summer results in fires in this vegetation. Communities in these areas of Australia are accustomed to regular cycles of bushfires, but changes to climatic conditions, including extensive droughts, are steadily increasing the devastating effects of these fires. When vast areas of potential fuel accumulate, bushfires can rage out of human control and cause widespread destruction (Blanchi et al., 2010). It is vitally important for Australian government bodies to gain detailed information on the frequency of extreme fire danger and devise critical mitigation and adaptation strategies to limit bushfires.

There are several indicators used to assess fire weather danger. One of Australia's most widely used fire danger indicators is the McArthur Forest Fire Danger Index (FFDI) (McArthur, 1967; Dowdy et al., 2009; Matthews, 2009). This index combines meteorological and fuel information; specifically, it uses dryness, based on rainfall and evaporation, and the meteorological variables: wind speed, temperature, and humidity. The long-term tendency of the fire weather danger can be quantified by calculating return periods (RP) of extremes of FFDI using extreme value distributions (Coles, 2001; Beirlant et al., 2004). Return Periods of the FFDI index will be used in this study to illustrate our bias-correction technique.

Climate simulations, including high-resolution simulations, have systematic biases when compared with observations. The reason for these biases is imperfect physical models, discretisation of continuous functions and averaging of calculations over grid cells

(Christensen et al., 2008; Ho et al., 2012; Wehner, 2010). For practical applications such as simulation-based fire weather danger mapping, it is necessary to correct those biases. Many bias correction methods are discussed in the literature (Teutschbein and Seibert, 2012; Bordoy and Burlando, 2013; Christensen et al., 2008). These methods can be classified as,

Linear correction:

- Multiplicative correction (Berg et al. 2012; Teutschbein and Seibert, 2012). This is the most straightforward technique for bias correction. The mean of the distribution is multiplied by a correction factor defined as the ratio of the mean of the observed distribution and the mean of the climate simulation.
- Additive correction (Berg et al. 2012). In this technique, the correction factor is the difference between the mean of the observed distribution and the mean of the simulations. The simulations are corrected by adding this factor to the mean of the distribution.
- Correction employing Q-Q plots (Déqué 2007; Bennet et al. 2011; Wilks 2006). This technique plots quantiles of observed vs simulated data corresponding to the same cumulative probability. If both distributions are similar, the quantiles will be plotted over a 45-degree diagonal. Off-diagonal location of the simulations represents the simulation bias. A correction factor to force the simulations to lie over the diagonal can easily be found. Other implementations of the Q-Q technique for bias-correction are presented in Enayati et al. (2020).

Non-linear correction:

- Using a standard distribution. The advantage of this technique is that unlike linear correction, which corrects only the mean, the use of a distribution corrects the simulations' variance. Teutschbein and Seibert (2012) use an exponential distribution. Ines and Hansen (2006) use a Gamma distribution.
- Variance scaling. The previous technique was developed for precipitation time series because of the use of exponential and gamma distributions. For correction of other time series, a more general technique, using the Gaussian distribution, was developed by Chen et al. (2011).
- Histogram equalisation. In this technique, a transfer function to shift the simulations to agree with the observations is found (Berg et al. 2012). For precipitation, the suitable distribution is the Gamma (Teutschbein and Seibert 2012), whilst for temperature, the suggested distribution is the Gaussian (Piani et al. 2010).
- Regression of station-based and climate-simulated values for the same grid. A cubic regression to consider location and elevation has been developed by Mannshardt-Shamseldin et al. (2010).

Most of the current studies for bias correction of climate-simulated data focus on the distribution's main body. Very few studies analyse bias correction of the extreme values located in the tail of the distribution, i.e. high values that have a very low probability of occurring, typically 1 in 100 years or more. In natural hazard studies, the quantities of interest are extreme values since mean values seldom pose a threat to human life or infrastructure. Comparison of observed and climate simulated daily climate extremes for five indices by Kiktev et al. (2003) shows that the difference between them can be significant, and it is not consistent for all regions of the world. Mannshardt-Shamseldin et al. (2010) compared station-based precipitation extremes with gridded data obtained from reanalysis and found that the former can be as high as three times the gridded data. Wörner et al. (2019) show that the bias in only one variable can significantly affect results downstream for processes that depend on several climatological variables.

These studies point towards the need for a robust methodology for bias-correction of extreme values in climate simulations. This paper presents a practical algorithm for bias correction of extreme values of climate simulated FFDI.

2. Data Utilised In This Study

The 'observed' or 'measured' data used in this study for bias correction is the historical fire weather datasets for Australia developed by Lucas (2010). These datasets cover 40 years from 1972 to 2011 and are based on measurements from 78 meteorological observing weather stations across Australia. Clarke et al. (2012) studied the quality of these data sets and found that only 38 of the 78 stations are considered of good quality. Within south eastern Australia (SEA), the region of interest in this study, there are 22 of these 38 quality stations; those are the stations selected for this study; their variables will be referred to as 'observed' or 'measured'.

The Climate Futures for Tasmania Project (CFT) generated the climate simulations utilised in this study (Corney et al. 2010). The CFT team dynamically downscaled six General Circulation Models using CSIRO's Conformal Cubic Atmospheric Model (CCAM) (McGregor et

al. 2001). They also generated high-resolution climate simulations forcing CCAM with the NCEP/NCAR reanalysis data (Kalnay et al. 1996). For this project, we utilise the latter.

Calculation of fire weather danger using high-resolution climate simulations offers several advantages over observation-based data:

- Climate models calculate the weather/synoptic-scale conditions over a regular grid over a long period. This gridded data can be used to calculate the spatial distribution of the FFDI.
- Climate modelled data allows researchers to study the future behaviour of extreme fire weather conditions including the impact of climate change on FFDI.
- Climate modelled data (unlike station observations) is free from recording errors, missing values, changes in the environment surrounding the stations, equipment failure, etc. Hence, more consistent results can be obtained.

The disadvantage of climate model data is accuracy when compared against observations. In practical applications, it is necessary to correct the bias to use climate simulations for risk analysis.

3. Model Description

This study quantifies natural hazard using the Average Recurrence Interval (ARI) or more commonly known as the Return Period (RP) of the event. If a given value of the event, termed 'return level', is exceeded with probability 'p' on average once a year, the RP corresponding to this return level is 1/p years (Coles 2001). For instance, if the average annual probability of exceeding an FFDI of 50 at a particular location is 0.002, then 50 is the 500-yr RP of FFDI at the location, i.e. it is expected that an FFDI of 50 is exceeded, on average, once every 500 years. The concept of RP is particularly useful to assess the long-term likelihood of extreme values, the values of interest in hazard studies. In this case, we fit an extreme value distribution (EVD) to the tail of the data and calculate RP of FFDI for a range of years well beyond the number of years available in the dataset (Coles, 2001; Beirlant et al., 2004).

There are two basic methodologies to fit EVDs:

- The 'block maxima' method in which an extreme value distribution is fitted to the annual maxima. The distribution used in this case is the Generalised Extreme Value Distribution (GEV).
- The 'peaks-over-threshold' technique utilises all values over a given threshold to fit the distribution. In this case the distribution used is the Generalised Pareto Distribution (GPD). This methodology has several advantages over the 'block maxima' method; firstly it uses a lot more data to fit the distribution, and secondly, by setting the threshold high enough, the data will be better distributed in time, improving the likelihood that the data samples are independent from each other, one of the conditions of EVD modelling. This is the method recommended when maximum daily observations are available (Coles 2001; Holmes & Moriarty 1999)

3.1 Climate simulated RP of FFDI

To calculate the daily maximum FFDI from the climate simulations, we used an expression developed by Noble et al. (1980), which relates the local weather with the vegetation dryness (rainfall deficit) at a given region. The expression is given by,

FFDI = 2*exp (0.987*ln (DF) − 0.0345*RH + 0.0338*T + 0.0234*WS − 0.45) (1)

where: DF = Drought factor (rainfall deficit)

RH = Relative humidity (%)

T = air temperature (°C) around 1.5–2m above the ground level

WS = wind speed (km/h) at 10 metre height

We used the maximum daily screen-level temperature and the surface level relative humidity (RH) at 06 hours UTC time for this study. The CFT simulations calculate RH at 6-hour intervals; we selected RH at 06 hours UTC, which correspond to 4 PM (EST) in south eastern Australian states because at around this time of the day, RH tends to be lowest, and hence the FFDI tends to peak (Lucas et al. 2007). For wind speed, we extracted the maximum daily 10m height over open, flat terrain.

To improve accuracy in the modelled data, we use observed DF calculated by the Australian Bureau of Meteorology (BoM) from its network of stations (Finkele et al. 2006). The DF dataset covers the whole country on a 0.25x0.25-degree grid for the period 1965–2006.

For calculation of FFDI we re-gridded the DF to a 0.5x0.5-degree grid.

Return periods of FFDI for a wide range of years were calculated. Since we have maximum daily FFDI we used the 'peaks-over-threshold' technique. The procedure to select the appropriate threshold to fit the GPD in wind applications is discussed in Sanabria and Cechet (2007). In this procedure, the threshold which produces the highest bound RP curve is selected. This is because maximum daily values of natural phenomena such as wind speed, temperature, or precipitation peak in nature. FFDI, on the other hand, is an indicator of fire weather conditions calculated from four climatic variables using an exponential distribution as shown in Eq. (1). In most of the stations considered in this paper, the RP curve of FFDI is not bounded (i.e. it does not asymptote to a finite value, see Fig. 2). Consequently, the bounded condition cannot be imposed on the climate simulated FFDI dataset. For consistency the condition was relaxed for all stations to fit unbounded GPDs to the FFDI data. The appropriate threshold to fit the GPD was then selected as the average of the thresholds used to calculate the RPs of observed FFDI at the 38 quality recording stations, which is 0.4 of maximum FFDI at the station (Sanabria et al. 2013).

For calculating the Return Periods for the 2242-cell grid, we extracted data from the simulations for a 30-yr period starting in 1965 (to match the DF data provided by BoM). The period 1965−1994 was selected because we want to study the fire weather hazard under current climate conditions. On the other hand, a minimum of 30 years is recommended because it provides enough extreme values for a good fitting of the distribution (Palutikof, 1999; Cechet et al. 2012).

In McArthur's original calculation, the FFDI value was calibrated to have a maximum of 100 for what was considered the worst possible fire weather conditions in Australia (McArthur 1966). However, this value has since been exceeded in severe to extreme fire weather situations. Therefore, for this work, we use the unbounded value calculated by Eq. (1) rather than truncating it at 100.

4. Results
4.1 Station-based RP of FFDI

Meteorological recording stations where long-term measurements of the parameters described in Sect. 3.1 are available allow for a detailed comparison of measured and modelled RP of FFDI. The suitable recording stations located in the south eastern part of Australia are shown in Fig. 1 (Lucas 2010); see also Table 1. Four stations within this region were used to illustrate the methodology; they are located at the Brisbane, Canberra, Mildura, and Ceduna airports. Figure 2 shows the curves of 10 to 1000-year RP of observed and modelled FFDI at these stations. The modelled data was extracted from the grid where the station is located. The difference (bias) between observed and modelled RP as a percentage of the former is presented in Table 1: column 2 shows the bias for the 50-yr RP ("Original bias RP50"), and column 3 shows the bias for the 100-yr RP ("Original bias RP100"). We can see that the former's maximum value is 44.4%, whilst the maximum bias for the 100-yr RP is 46.5%; they are significant biases indeed.

Comparing these RPs of observed and modelled FFDI and those of other observing stations (presented in the Supplementary Material, see the Appendix) shows that the calculations using climate simulations produce lower RP curves than those using observed values.

4.2 Map of RP of FFDI

The spatial distribution of fire weather hazard in Australia was assessed by Sanabria et al. (2013).

They calculated RPs of measured FFDI at several recording stations around Australia using Lucas' datasets. These RPs were then interpolated to a 0.5x0.5-degree grid, using different spatial interpolation algorithms in order to present the information in the form of maps. The best results were obtained using a hybrid of Random Forest and Inverse Distance Weighting, termed RFIDW (Li et al. 2011). Figure 3a shows the 50-year RP of measured FFDI generated by spatial interpolation (using RFIDW); it will be used as the benchmark in this study.

Figure 3b shows the 50-year return period of FFDI calculated from the climate simulations. Note the empty polygons in Australia's central and western parts in the climate-simulated map; BoM's DF datasets do not include values in these regions.

Both maps show regions of very high FFDI in the southwest near the border between SA and WA: in the map of measured data, these values reach 180 while the simulation-based map shows FFDI values of 190. Similarly, the southern part of SA shows values of 180, while this value in the simulations is 170. There is a significant bias in the simulations to this region's right (north of Adelaide): the observations show a region of 170 FFDI, while in the simulations, this region reaches only 80. A similar situation can be observed in southern Vic: the

observations show an FFDI of 100 while the simulations show values between 60 and 70. The bias is even higher in western Vic; the observations show an FFDI of 160 while the simulations show values of 90.

Another high bias region is southwest QLD and northwest NSW, where the simulations show an FFDI of 120 while the observations show values of 180. The most significant mismatch between both maps is, however, in the coastal areas of Eastern Australia, where the climate simulations project maximum values of around 50 while the benchmark shows values of around 120. Note the low values projected by the simulations in the ACT region (southeast NSW) compared with the benchmark. Also note the mismatch in Tasmania; the benchmark shows relatively high FFDI values (around 80) in southeast Tasmania and low values in the western part of the State; the simulations project lower values in the whole of Tasmania.

5. Bias-correction Methodology

As discussed above, for an appropriate calculation of the RP of climate modelled FFDI, it is necessary to correct the bias of the FFDI. A two-step bias-correction algorithm for climate

modelled FFDI was developed as follows:

Step 1. Correction of the main body of the distribution. This step is carried out based on the Q-Q plot shown in Fig. 4. This plot shows that climate simulated FFDI values are lower than the measured ones, especially at high values. A multiplicative correction factor (MCF) to increase the climate-simulated FFDI in order to match the measured FFDI can be found. As explained in Sect. 1, this is a simple yet compelling technique widely used in climate simulations (Enayati et al. 2020; Bennett et al. 2011). The appropriate MCF for this case is given by the ratio of the mean of the observed FFDI and the mean of the climate simulated FFDI,

MCF = mean(obs_FFDI)/mean(simulated_FFDI) (2)

The MCF for this plot was found to be 1.4; the simulated FFDI distribution is then multiplied by this MCF. This procedure provides an improvement to the calculation of FFDI, especially for low values, as can be seen by comparing Figs. 4 and 5a. However, the RP depends on extreme values, i.e. the tail of the distribution; therefore, it is necessary to correct its tail to improve the RP calculation substantially. Figure 5a shows that the corrected quantiles' main body lies on the 45-degree line, indicating a good agreement with the observations. Still, the tail of the distribution (values over a FFDI of 41 indicated by the blue line) shows a considerable bias. Therefore it is necessary to implement a second correction step targeting the tail of the FFDI distribution.

Step 2. Correction of the tail of the distribution. Again, we will use multiplicative factors to correct only the tail of the distribution: values of climate-simulated FFDI over the vertical (blue) line shown in Fig. 5a were extracted. By definition, extreme values are rare events, and hence it is necessary to select only a few samples from the tail of the distribution; in most cases, about 30 or 40 samples out of the 10943 are enough. These many samples correspond to about the 99 percentile. Table 1 columns 5 and 6 show the number of tail samples selected and the corresponding percentile for the stations used in this study.

A correction factor for these 'n_T' samples was calculated as the ratio of the observed and simulated FFDI, that is,

tail_BCF$_i$ = obs_FFDI$_i$/simulated_FFDI$_i$ for i = 1,2... n_T (3)

The n_T top simulated FFDI values were then corrected by multiplying them by these correction factors.

Figure 5b shows the Q-Q plot of observed and corrected simulated FFDI after implementing the two-step correction procedure on the simulated FFDI. Figure 5b shows an excellent agreement in both the main body and the tail of the FFDI distribution. The corresponding curves of RP of simulated FFDI were calculated from the corrected FFDI. Figure 6 presents the curves of RP of FFDI calculated using measured FFDI (black), non-corrected climate simulated FFDI (red) and two-step corrected climate simulated FFDI (blue). The difference between observed and two-step corrected modelled RP (as a percentage of the former) is shown in Table 1, columns 8 and 10. Column 8 is the bias between observed and corrected modelled RP50, and column 10 is the bias for RP100.

Figure 6 shows a close match between the RP curves of observed and bias-corrected simulated FFDI at most stations. In all cases, the calculation of RP of FFDI using bias-corrected simulated FFDI shows a substantial improvement when compared against observations. Note, however, that the improvement is not uniform across all stations; in Mildura and Ceduna, there is a perfect match of simulated and observed FFDI, whilst in Brisbane and Canberra, there is a small difference between the corrected RP and the measured RP curve at the range of interest in this study: 50 and 100 years. Figure 6 shows that the two-step bias correction procedure produces good results. The

improvement factor for the 50-yr RP is given by the ratio of the climate-corrected simulations and the non-corrected simulations; for the Brisbane case, this factor is 1.63. Similarly, the corrected and non-corrected 100-yr RP ratio gives BCF2_100, the total bias correction factor for a 100-yr RP of FFDI using climate simulations; for Brisbane, this factor is also1.63.

Table 1 columns 7 and 9 show the improvement factor for the 50 and the 100-yr RP of FFDI at each station (total two-step bias correction factor, named "BCF2_50" and "BCF2_100", respectively). Curves of corrected RP for the other stations are presented in the Supplementary Material; see the Appendix. Column 8 compares the bias-corrected 50-yr RP of FFDI with the corresponding 50-yr RP of the benchmark as a percentage of the latter ("Bias50"). Similarly, column 10 compares the 100-yr RP of FFDI and the benchmark ("Bias100"). With the correction, the maximum bias of the climate simulated 50-yr RP of FFDI is 5.23%, while the maximum bias for the modelled 100-yr RP of FFDI is 7.38%.

5.1 Bias-correction of the FFDI maps

From the discussion above, it is clear that the two-step bias correction algorithm improves the calculation of fire weather hazard using climate simulations. For most observing stations, this improvement was shown to be substantial as shown in Table 1. This correction was easy to implement at a station level where there is measured FFDI data, and hence a correction factor for climate simulated FFDI can be calculated. Correction of simulated FFDI at every cell of the grid is more problematic to implement because there are no observations to compare with. To calculate the two-step correction factor for each cell of the grid, a simple procedure was implemented based on the correction factors' interpolation (BCF2_50 and BCF2_100) shown in Table 1 columns 7 and 9. An Inverse Distance Weighting algorithm (IDW) was used for the interpolation. This is a versatile, easy to program and fairly accurate algorithm under a wide range of conditions (Li and Heap, 2014; Lam, 1983). To illustrate the technique, Fig. 7 shows the spatial distribution of BCF2_50 on SEA.

Table 1
Bias and Step1 and 2 bias correction factors for modelled FFDI.

Station	Original bias RP50 (%)	Original bias RP100 (%)	Step 1 Corrtn factor	Tail samples (n_T)	Pcntile	BCF2_50	CorrectedBias _RP50 (%)	BCF2_100	CorrectedBias_RP100 (%)
Adelaide	16.9	17.6	1.15	20	99.89	1.19	0.87	1.20	1.42
Amberley	41.8	43.0	1.54	22	99.80	1.71	0.70	1.72	2.09
Bendigo	12.9	17.2	0.85	36	99.23	1.15	0.18	1.20	0.64
Brisbane	40.6	41.8	1.40	34	99.63	1.63	3.22	1.63	5.08
Canberra	16.4	19.2	1.05	17	99.89	1.18	1.17	1.20	2.77
Ceduna	6.7	8.4	0.95	38	99.72	1.06	0.70	1.08	1.10
Charleville	12.2	13.6	1.00	65	99.40	1.11	2.20	1.12	2.93
Cobar	27.0	31.7	0.97	47	99.55	1.30	5.23	1.36	7.38
Cs Harbour	22.8	27.0	0.70	14	99.80	1.28	1.10	1.36	0.94
Hobart	25.8	28.0	1.05	16	99.86	1.34	2.13	1.35	4.60
Launceston	7.8	5.6	1.20	29	99.88	1.06	2.40	1.04	1.80
Laverton	42.6	46.5	0.90	23	99.97	1.79	1.47	1.88	2.99
Melbourne	9.8	11.6	0.95	60	99.33	1.07	3.01	1.09	3.53
Mildura	15.0	18.6	0.90	62	99.98	1.17	0.11	1.22	0.98
Moree	44.8	46.6	1.20	22	99.10	1.84	2.16	1.90	2.28
M Gambier	19.7	24.4	0.90	14	99.97	1.22	1.67	1.30	1.74
Nowra	44.4	46.4	1.30	22	99.50	1.80	0 .00	1.86	0.00
Sale	16.3	21.9	0.95	7	99.94	1.17	1.88	1.27	1.17
Sydney	10.2	11.5	0.95	25	99.89	1.09	2.46	1.11	2.07
Wagga	5.1	7.6	1.00	11	99.99	1.04	1.37	1.06	1.62
Williamtn	18.2	22.3	0.80	47	99.50	1.22	0.77	1.29	0.52
Woomera	4.2	4.53	1. 00	24	99.83	1.02	2.49	1.02	2.75

Using these gridded correction factors, it is possible to improve the simulation-based map of the 50-yr RP of FFDI originally shown in Fig. 3b. To facilitate visual comparison, Fig. 8 shows on the same graph Figs. 3a (50-yr RP of measured FFDI, our benchmark), 3b (50-yr RP of non-corrected simulations) and the 50-yr RP of corrected FFDI, Fig. 8c.

Comparing Figs. 8c and 3b (now 8b), we can see a substantial improvement of the map, especially in eastern Australia's coastal area. In the map shown in Fig. 8b, most of these coastal areas reach a maximum FFDI of about 40, while in map 8c, the maximum of this coastal area varies between 70 and 100, a more realistic figure compared with 8a. The same can be said about northern Victoria; map 8a shows maximum values of about 150, which are matched in map 8c, while these values in map 8b are about 80. Southern and eastern Vic has also been improved.

Map 8c shows high values of FFDI in southern Tasmania. Similarly, the high FFDI values of the ACT region (southeast NSW) shown in map 8a, which were missing in map 8b, are now visible in map 8c.

In general, we can see a 50-yr RP map that is closer to the benchmark. There are, however, some limitations; the algorithm tends to overcorrect some regions: the values of FFDI on the border between WA and SA are too high. The high values of FFDI located over south QLD-Northern NSW are located much lower and cover a wider region, while the region of high values over southeast SA (close to the Vic border) is missing in map 8c. In Tas, the corrected map shows high FFDI values in the southern part of the State but misses the eastern part's high values.

A source of error in this technique is its dependency on interpolation. The overcorrection of the border between WA and SA happens because there are no stations to help interpolate these regions. Hence the interpolation of the two-step correction factors for these regions depend on stations located further away in SA and Vic, which have higher FFDI values as shown in Fig. 7. The technique should give better results in regions with a higher density of recording stations.

To finish off this paper, Fig. 9 presents the map of 100-yr RP of FFDI using interpolation of measured FFDI and the corresponding map of climate simulated 100-yr RP corrected using the procedure given above. The corrected climate simulated map of 100-yr RP looks very similar in most regions showing that the algorithm can correct the bias of extreme values of climate simulations and improve the calculation of RPs. As explained before, the significant bias in south WA and southwest SA is due to limitations in interpolating the two-step bias correction factors.

To overcome the limitations of the technique presented here, several interpolation algorithms for the two-step bias correction factors were tested; unfortunately, none of them improved map 8c. Another experiment doing interpolation of only step 1 of the bias correction process (column 4 of Table 1) was also tried out; these experiments did not improve the results presented in this paper and were discarded (these maps are presented in the Supplementary Material, see the Appendix).

6. Conclusions And Future Work

A two-step bias correction algorithm to improve RP calculation of climate simulations has been presented in this paper. RP calculation depends on the simulations' extreme values, and hence the algorithm corrects both the main body and the extreme values of the simulated data. RPs are a fundamental tool to calculate the hazard posed by natural phenomena. To illustrate the technique, we calculated the RP of fire weather hazard in southeast Australia.

Fire weather hazard was assessed by employing extreme value statistics to calculate return periods of the McArthur Forest Fires Danger Index (FFDI) at each of the model grid points. The initial return period modelled FFDI results were validated against observations from a number of meteorological recording stations in Australia with quality long-term FFDI datasets. The comparison showed that the observation and the climate-modelled FFDI have similar fire weather danger patterns for southeast Australia. Still, the modelled estimates of FFDI show substantial differences in most stations.

The primary source of bias in these types of studies is in the components of the FFDI calculation. The components of FFDI are calculated as cell averages while the observed variables are recorded at a point (station). Using a two-step bias-correction procedure - appropriate for location-based FFDI calculations - it was possible to improve the modelled FFDI estimates substantially. The bias in calculating the 50-year RP of corrected FFDI extends over the range 0 to 5.23% (for the 22 observing stations considered), indicating a good match between observed and bias-corrected simulations. The procedure is, however, inappropriate for direct correction of gridded FFDI. In this case, we used a spatial interpolation algorithm to give a spatial texture to the FFDI correction factors. The gridded FFDI calculation was improved by adjusting the simulated FFDI with this spatially distributed correction factor.

Availability of a robust procedure for bias correction of climate simulations will allow planning and emergency authorities to assess future fire weather danger in Australia using projections of climate simulated FFDI. This is important to reduce the bushfire risk in regions of serious fire weather danger. We are working on a project to study FFDI in Australia under future climate conditions.

Appendix

Interested readers can see more plots of the procedures discussed in this paper in the Supplementary Material as follows:

File Description

"All_orig_QQplt_stn_FFDI.pdf" It shows the QQplots of obs and modelled FFDI before any correction is implemented, i.e. it is Fig. 4 for all stations.

"All_bcsteps1_2_QQplt_FFDI.pdf" It shows QQplots of obs and modelled FFDI after steps 1 and 2 have been implemented, i.e. it is Fig. 5b for all stations.

"All3_RP_FFDI.pdf" It contains the curves of RP of obs FFDI, non- corrected climate simulated FFDI; and two-step bias corrected FFDI, i.e. it is Fig. 6 for all stations.

"BCF2_compare_interp.pdf" Comparison of maps of 50-yr and 100-yr RP using two-step and one-step bias correction. The interpolation of the correction factors is carried out by different interpolation techniques.

Declarations

References

Abram NJ, Henley BJ, Sen Gupta A, Lippmann TJR, Clarke H, Dowdy AJ, Sharples JJ, Nolan RH, Zhang T, Wooster MJ, Wurtzel JB, Meissner KJ, Pitman AJ, Ukkola AM, Murphy BP, Tapper NJ and Boer MM (2021) Connections of climate change and variability to large and extreme forest fires in southeast Australia. Communications Earth & Environment 2, 8.

Australia Institute for Disaster Resilience (2020). Accessed 9 March 2021, https://knowledge.aidr.org.au/resources/black-summer-bushfires-nsw-2019-20/

Beirlant J, Goegebeur Y, Segers J, Teugels J (2004) Statistics of Extremes: Theory and Applications. John Wiley & Sons.

Bennett JC, Grose MR, Post DA, Ling FLN, Corney SP, Bindoff NL (2011) Performance of quantile-quantile bias-correction for use in hydroclimatological projections. Proc. 19th Int. Congress on Modelling and Simulation (MODSIM2011). Perth.

Berg P, Feldmann H, Panitz HJ (2012) Bias correction of high-resolution regional climate model data. Journal of Hydrology 448–449, 80–92

Blanchi R, Lucas C, Leonard J, Finkele K (2010) Meteorological conditions and bushfire-related house loss in Australia. Int. J. of Wildland Fire, 19, 914-926.

Bordoy R, Burlando P (2013)   Bias Correction of Regional Climate Model Simulations in a Region of Complex Orography. Journal of Applied Meteorology and Climatology. Vol 5, pp82-101.

Cechet RP, Sanabria LA, Divi CB, Thomas C, Yang T, Arthur WC, Dunford M, Nadimpalli K, Power L, White CJ, Bennett JC, Corney SP, Holz GK, Grose MR, Gaynor S, Bindoff NL (2012) Climate Futures for Tasmania: Severe wind hazard and risk. Technical Report. Geoscience Australia Record 2012/43. GeoCat   74052.

Chen C, Hagemann JO, Piani C (2011) On the contribution of statistical bias correction to the uncertainty in the projected hydrological cycle. Geophys. Res. Lett. 38 (L20403), 6.

Christensen JH, Boberg F, Christensen OB, Lucas-Picher P (2008) On the need for bias correction of regional climate change projections of temperature and precipitation. Geophysical Research Letters 35, L20709. DOI: 10.1029/2008GL035694.

Clarke HG, Lucas C, Smith (2012) Changes in Australian fire weather between 1973 and 2010, International   Journal of Climatology, DOI: 10.1002/joc.3480.

Coles S (2001) An Introduction to Statistical Modeling of Extreme Values. London: Springer.

Corney SP, Katzfey J, McGregor J, Grose MR, Bennett J, White CJ, Holz G, Gaynor SM, Bindoff NL (2010) Climate Futures for Tasmania technical report: climate modelling. Antarctic Climate and Ecosystems Cooperative Research Centre, Hobart, Tasmania.

Déqué M (2007) Frequency of precipitation and temperature extremes over France in an anthropogenic scenario: Model results and statistical correction according to observed values. Global and Planetary Change 57, 16-26.

Dowdy AJ, Mills GA, Finkele K, de Groot W (2009) Australian fire weather as represented by the McArthur Forest Fire Danger Index and the Canadian Forest Fire Weather Index. The Centre for Australian Weather and Climate Research, CAWCR Technical Report No. 10.

Enayati M, Bozorg-Haddad O, Bazrafshan J, Hejabi S (2020) Bias correction capabilities of quantile mapping methods for rainfall and temperature variables. Journal of Water and Climate Change. Pre-print May 2020, doi: 10.2166/wcc.2020.261

Finkele K, Mills GA, Beard G, Jones DA (2006) National Daily Gridded Soil Moisture Deficit and Drought Factors for Use in Prediction of Forest Fire Danger Index in Australia. Bureau of Meteorology Research Centre, Research Report No 119.

Handmer, J., Dovers, S. and Downing, T. (1999) Societal Vulnerability to Climate Change and Variability. Mitigation and Adaptation Strategies for Global Change 4, 267–281

Ho CK, Stephenson DB, Collins M, Ferro C, Brown SJ (2012) Calibration Strategies. A source of additional uncertainty in climate change projections. 'In Box', American Meteorological Society. DOI:10.1175/2011BAMS3110.1

Holmes JD, Moriarty WW (1999) Application of the Generalised Pareto Distribution to extreme value analysis in wind engineering. Journal of Wind Eng. and Industrial Aerodynamics 83, 1-10.

Ibarrarán, ME, Ruth M, Ahmad S and London M (2009). Climate change and natural disasters: macroeconomic performance and distributional impacts. Environment, Development and Sustainability 11, 549–569

Ines AVM, Hansen JW (2006) Bias correction of daily GCM rainfall for crop simulation studies. Agricultural and Forest Meteorology 138, 44–53

Insurance Council Australia (2020), accessed 9 March 2021, https://disasters.org.au/current-catastrophes/2019/11/13/november-bushfires.

Kalnay EM, Kanamitsu R, Kistler R, Collins D, Deaven L, Gandin M, Iredell M, Saha S, White J, Woollen J, Zhu Y, Chelliah M, Ebisuzaki W, Higgins W, Janowiak J, Mo KC, Ropelewski C, Wang J, Leetmaa A, Reynolds R, Jenne R, Joseph D (1996) The NCEP/NCAR 40-year Reanalysis Project. Bull. Amer. Meteor. Soc. 77, 437-471.

Kiktev D, Sexton D, Alexander L, Folland CK (2003) Comparison of modelled and observed trends in indices of daily climate extremes. Journal of Climate. Vol 16, 3560-3571.

Lam NS (1983) Spatial interpolation methods review. The American Cartographer 10, 129-149.

Li J, Heap AD, Potter A, Daniell J (2011) Application of machine learning methods to spatial interpolation of environmental variables. Environmental Modelling & Software 26, 1647-1659.

Li J, Heap AD (2014) Spatial interpolation methods applied in the environmental sciences: A review. Environmental Modelling & Software 53, 173-189.

Lucas C, Hennessy K, Mills G, Bathols J (2007) Bushfire Weather in Southeast Australia: Recent Trends and Projected Climate Change Impacts. Bureau of Meteorology Research Centre. Report to the Climate Institute of Australia.

Lucas C (2010) On developing a historical fire weather dataset for Australia. Australian Meteorological and Oceanographic Journal 60:1-14.

Mannshardt-Shamseldin EC, Smith RL, Sain SR, Mearns LO, Cooley D (2010) Downscaling Extremes: A Comparison of Extreme Value Distributions in Point-Source and Gridded Precipitation Data. The Annals of Applied Statistics. Vol. 4, No. 1, 484-502. DOI: 10.1214/09-OAS287.

Matthews S (2009) A comparison of fire danger rating systems for use in forests. Australian Meteorological and Oceanographic Journal 58, 41-48

McArthur AG (1966) Weather and grassland fire behaviour. Leaflet No 100. Forest Research Institute, Forestry & Timber Bureau. Canberra.

McArthur AG (1967) Fire behaviour in eucalypt forests. Commonw. Aust. Forest and Timber Bureau. Leaflet No. 107,

McGregor JL, Dix MR (2001) The CSIRO Conformal-Cubic Atmospheric GCM. Proc. IUTAM Symposium on Advances in Mathematical Modelling of Atmosphere and Ocean Dynamics.

Noble IR, Bary GAA, Gill AM (1980) McArthur's fire danger meters expressed as equations. Australian Journal of Ecology 5, 201 – 203.

Orr HG, Ekström M, Charlton MB, Peat KL and Fowler HJ (2021) Using high-resolution climate change information in water management: a decision-makers' perspective. Philosophical Transactions of the Royal Society A. 379

Palutikof JP, Brabson BB, Lister DH, Adcock ST (1999) A Review of Methods to Calculate Extreme Wind Speeds. Meteorol. Appl. 6, 119132.

Piani C, Weedon GP, Best M, Gomes SM, Viterbo P, Hagemann S, Haerter JO (2010) Statistical bias correction of global simulated daily precipitation and temperature for the application of hydrological models. Journal of Hydrology 395, 199–215

Sanabria LA, Qin X, Li J, Cechet R.P, Lucas C (2013) Spatial Interpolation of McArthur's Forest Fires Danger Index across Australia: Observational Study. Environmental Modelling & Software 50, 37-50.

Sanabria LA, Cechet RP (2007) A Statistical Model of Severe Winds. Geoscience Australia. GeoCat # 65052.

Smit B, Burton I, Klein RJT, Wandel J (2000) An Anatomy of Adaptation to Climate Change and Variability. In: Kane SM, Yohe GW (eds) Societal Adaptation to Climate Variability and Change. Springer, Dordrecht.

Teutschbein C, Seibert J (2012) Bias correction of regional climate model simulations for hydrological climate-change impact studies: review and evaluation of different methods. Journal of Hydrology 456-457, 12-29.

Van Aalst, M.K. (2006), The impacts of climate change on the risk of natural disasters. Disasters, 30: 5-18. https://doi.org/10.1111/j.1467-9523.2006.00303.x

Wehner M (2010) Sources of uncertainty in the extreme value statistics of climate data. Extremes 13:205-217.

Wilks (2006) Statistical Methods in the Atmospheric Sciences. 2nd Ed. Academic Press. Elsevier.
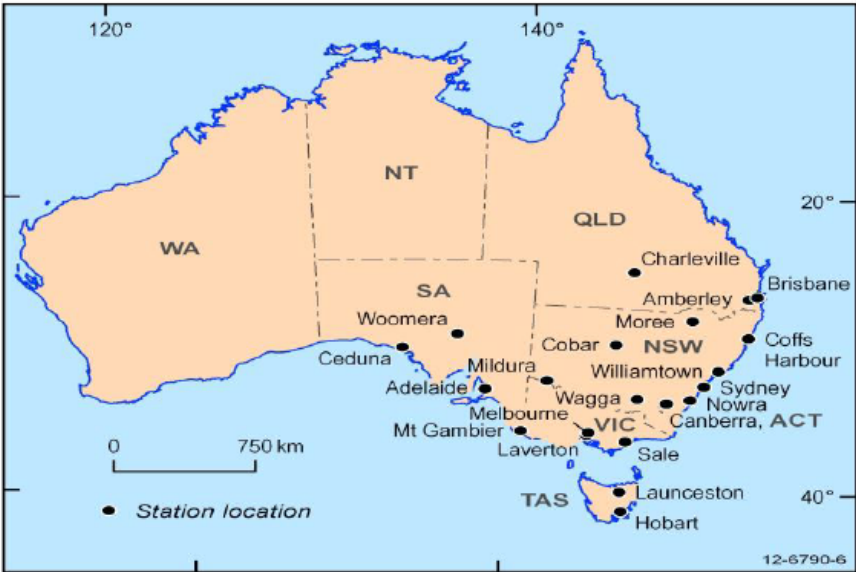
Figures

Figure 1

Location of selected meteorological recording stations in south-eastern Australia where suitable long-term FFDI data was available.
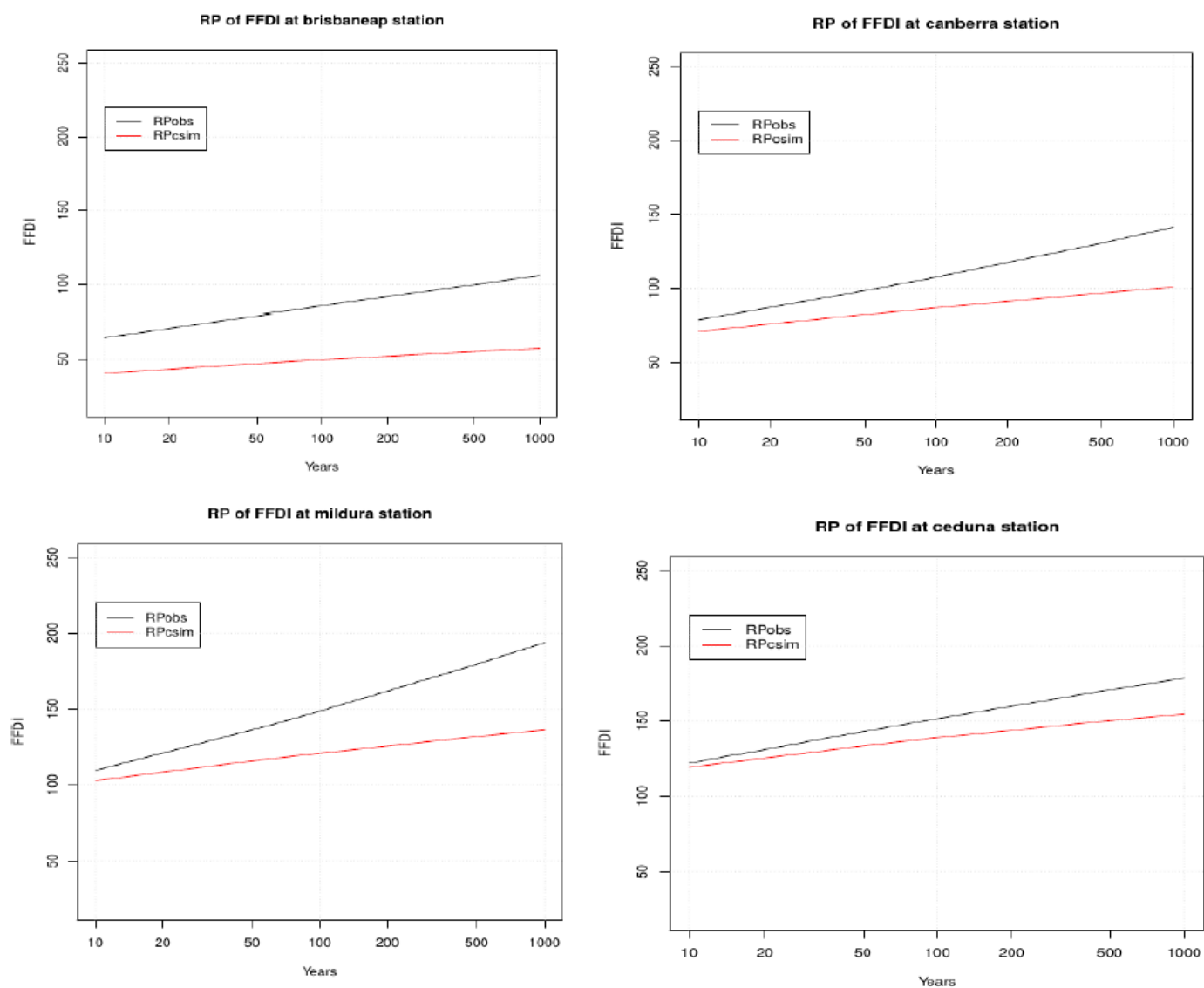
Figure 2

RP of FFDI at Brisbane, Canberra, Mildura, and Ceduna Airport stations. The black curve is the RP of observed FFDI; the red curve is the RP calculated from the simulations.
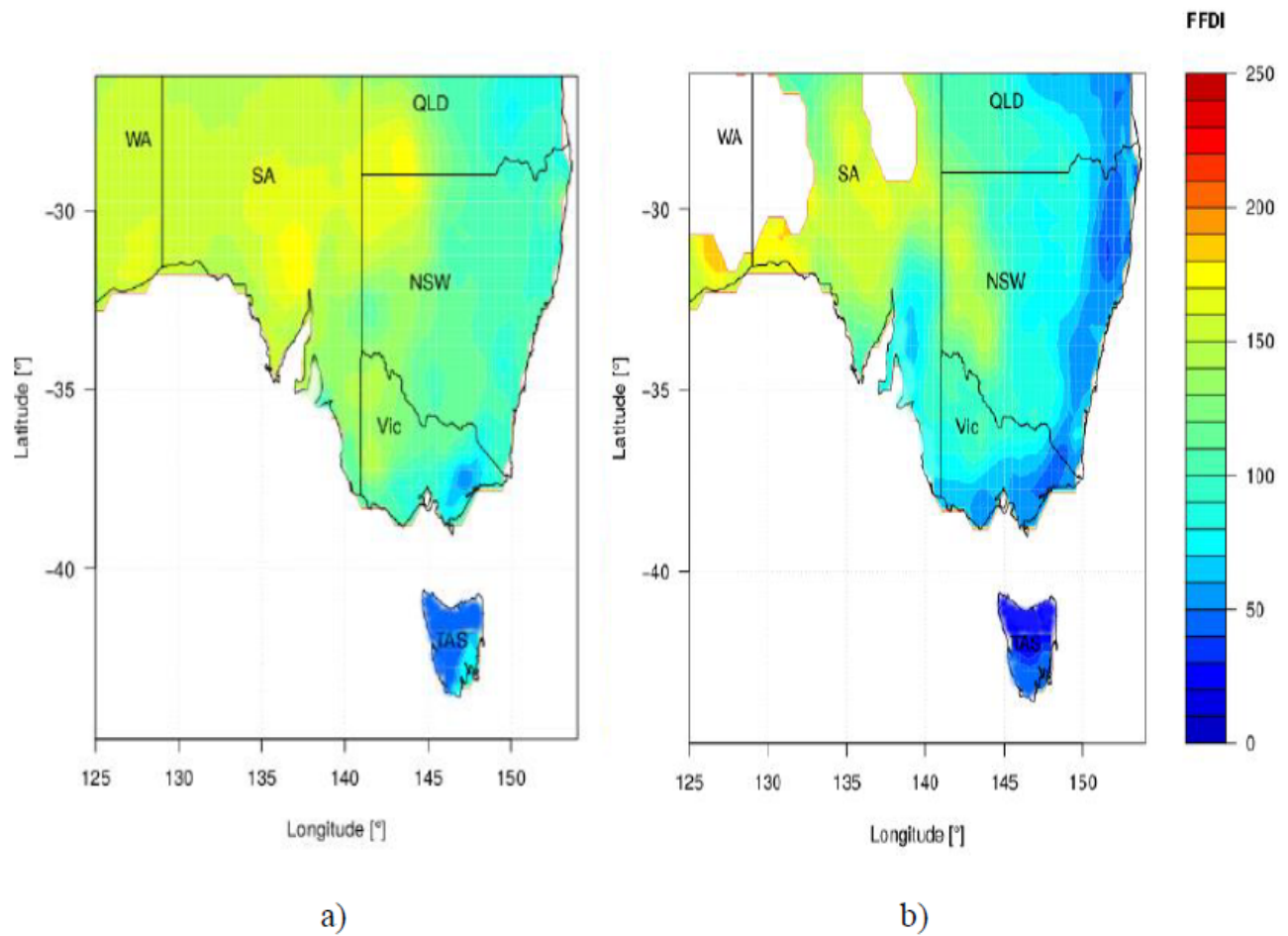
a)   b)

Figure 3

50-year RP of FFDI in southeast Australia calculated using a) interpolation of observations (via RFIDW) and b) climate simulations.
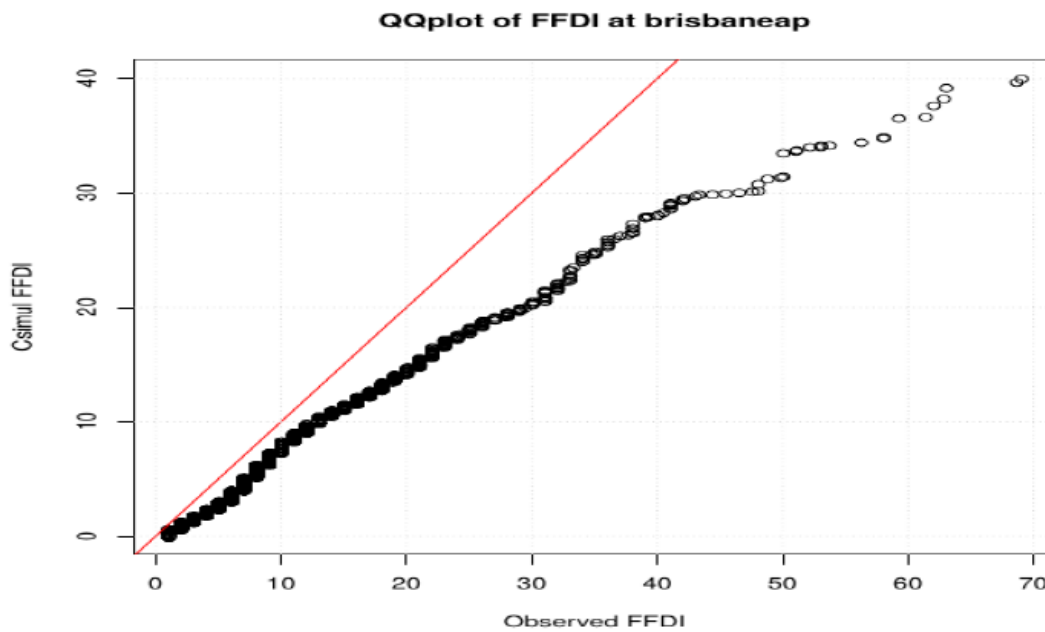
Figure 4

Q-Q plot of obs and simulated FFDI at Brisbane Airport station.

QQplot of FFDI at brisbaneap

Step1 correction factor = 1.4

a)

QQplot of corrected FFDI at brisbaneap

Two_step correction of simulated FFDI
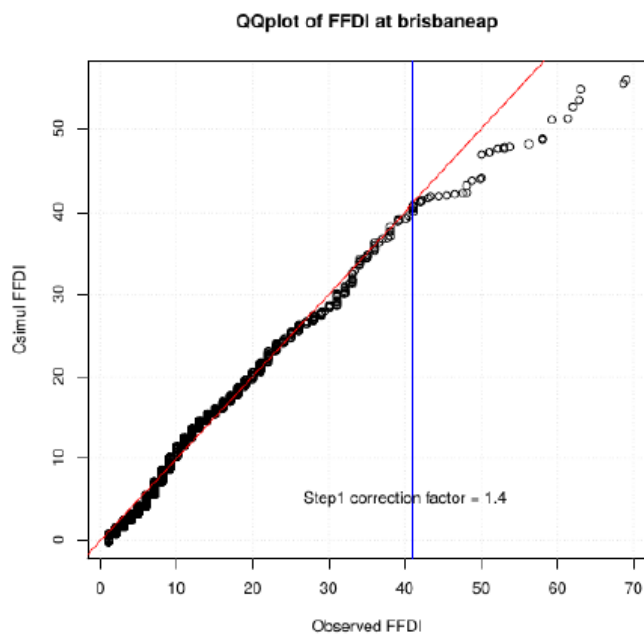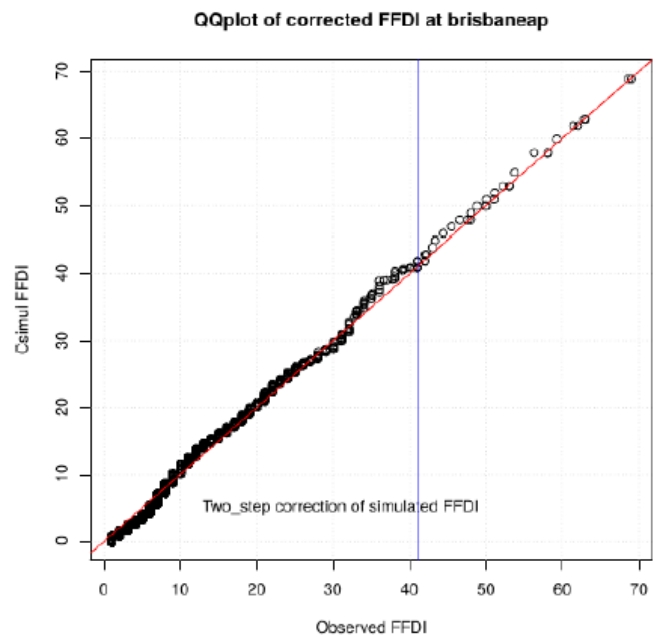
b)

Figure 5

a) Correction of the main body of the FFDI distribution, and b) Correction of the tail of the FFDI distribution for Brisbane Airport station.
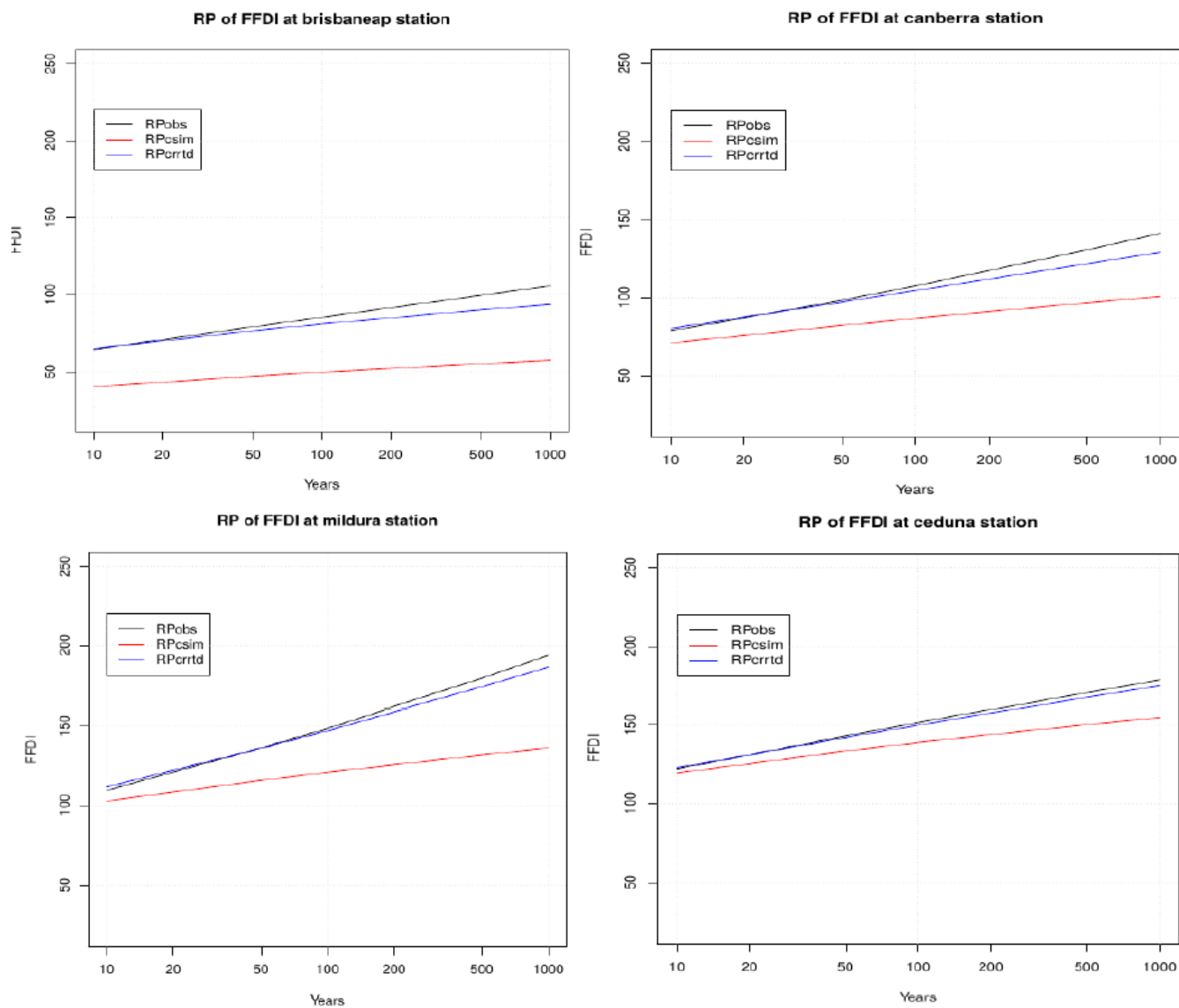
Figure 6

Curves of measured ("RPobs", black line), non-corrected ("RPcsim", red line), and corrected modelled RP ("RPcrrtd", blue line) of FFDI at Brisbane, Canberra, Mildura, and Ceduna stations.
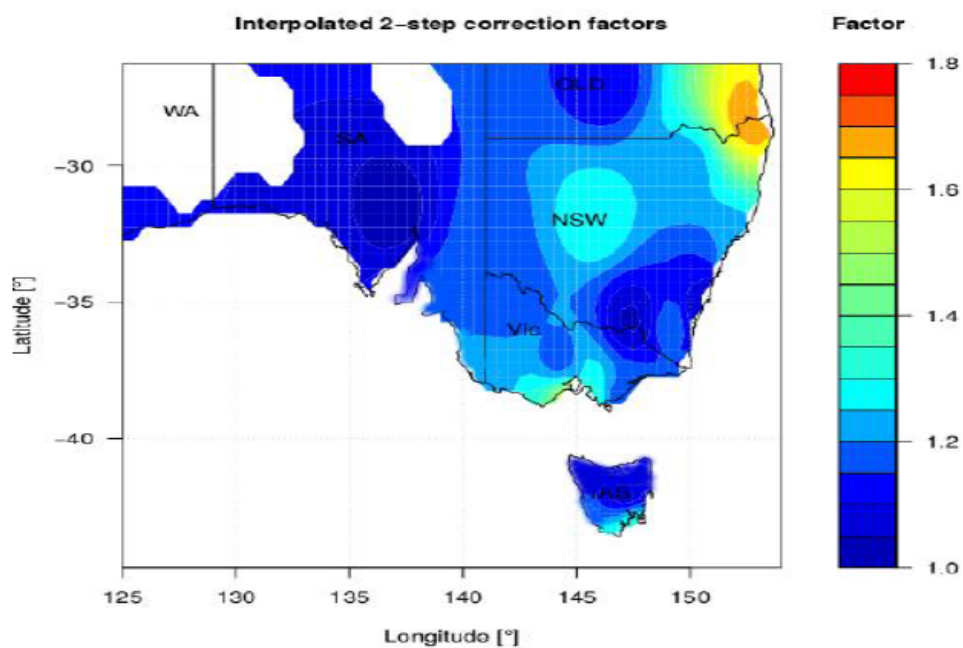
Figure 7

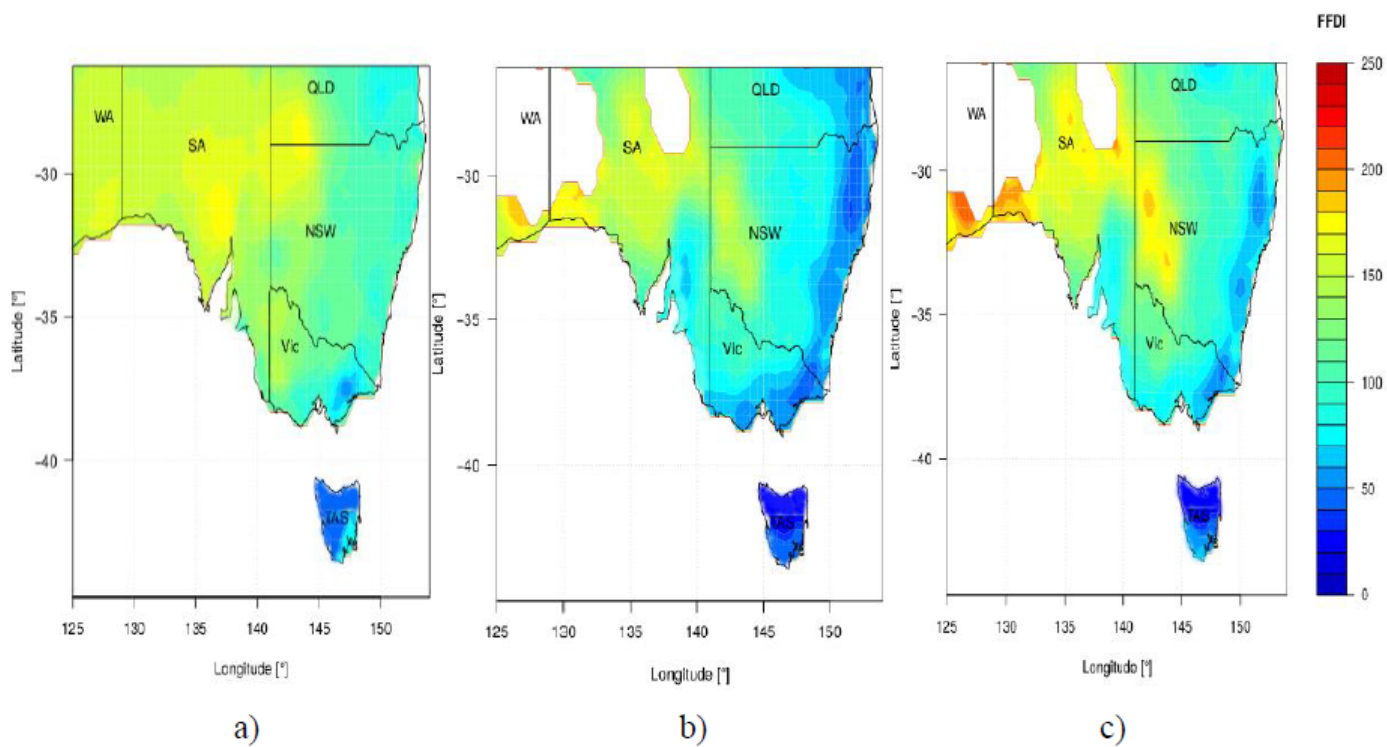Spatial interpolation of correction factors BCF2_50.

Figure 8

a) Map of the 50-yr RP of measured FFDI. b) Map of the 50-yr RP of non-corrected climate simulation. c) Map of the 50-yr RP of corrected climate simulation.
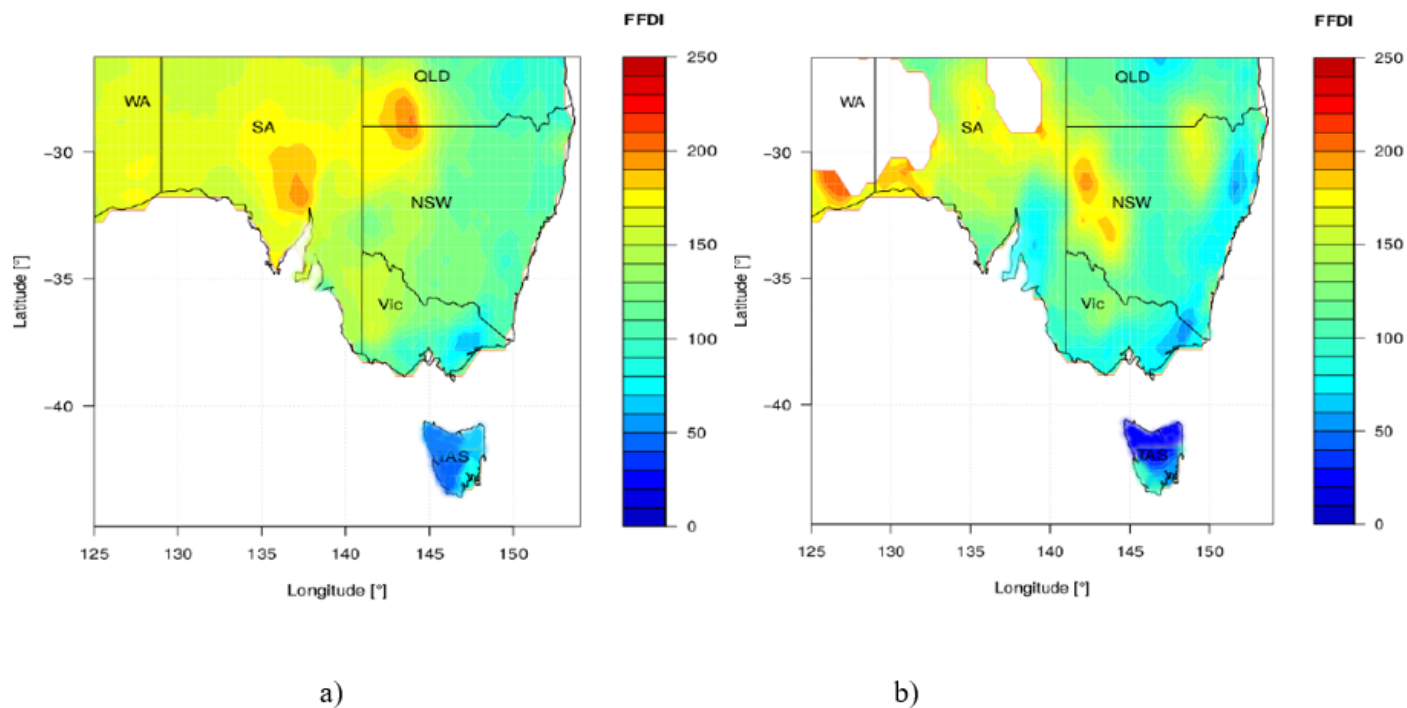
Figure 9

a) Map of the 100-yr RP of measured FFDI. b) Map of the 100-yr RP of corrected climate simulated FFDI

Supplementary Files

This is a list of supplementary files associated with this preprint. Click to download.

- All3RPFFDI.pdf
- Allbcsteps12QQpltFFDI.pdf
- AllorigQQpltstnFFDI.pdf
- BCF2compareinterp.pdf